IEEE Robotics and Automation Letters (RA-L) paper, presented at ICRA 2024, Yokohama, Japan. Cite as RA-L paper.

Combining Tail and Reaction Wheel for Underactuated Spatial Reorientation in Robot Falling With Quadratic Programming

Xiangyu Chu, Shengzhi Wang, Raymond Ng, Chun Yin Fan, Jiajun An, and K. W. Samuel Au

***Abstract*—Inertial appendages (e.g., tails and reaction wheels) have shown their reorientation capability to enhance robots' mobility while airborne or improve robots' safety in falling. The tail, especially with two Degrees of Freedom (DoFs), is normally subject to its limited Range of Motion (RoM). Although the reaction wheel circumvents this limitation, its efficiency has been shown lower than the tail in terms of inducing Moment of Inertia (MoI). In literature, only one type of inertial appendages has been used on terrestrial robots in the air, e.g., either using a tail on the hexapedal robot RHex or using a reaction wheel on the jumping quadruped robot SpaceBok. In this paper, to benefit from both unlimited RoM and efficient MoI-inducing, we propose combining a 1-DoF tail and a reaction wheel together for spatial reorientation (regulating the robot body's 3D orientation). Inspired by this, a hybrid tail-wheel robot is built, i.e., the tail that creates roll motion is attached to a wheel-equipped robot whose wheels act like a reaction wheel and generate pitch rotation; however, the robot is underactuated on the yaw rotation. To achieve its real-time spatial reorientation, we propose a novel quadratic programming algorithm based on a geometric metric for the underactuated hybrid tail-wheel robot. Within the proposed algorithm, the physical limitations on tail and wheel velocities are automatically accommodated. Numerical comparisons among wheel-wheel, tail-wheel, and 2-DoF tail robots showed the strength of the hybrid tail-wheel appendage on reorientation convergence and free of collision. Experimental results further demonstrated the capability of real-time spatial reorientation with underactuation and velocity constraints by using the combined tail-wheel inertial appendage.**

***Index Terms*—Biologically-Inspired Robots, Motion Control, Underactuated Robots, Quadratic Programming**

I. Introduction

Many terrestrial robots have shown incredible locomotion capabilities such as walking [1] and jumping [2]. Recently, researchers started to focus on their mobility in the air, aiming at achieving safe landing [3], [4] or demonstrating high agility [6], [7]. Except for a few robots relying on take-off angular momentum like Mini Cheetah's backflip [5], many robots' mobility performance in the air is heavily determined by reorientation capabilities. To enable such capabilities, applying inertia appendages is an effective way. These appendages can be tails, limbs, and even (reaction) wheels. Although various appendages exist, from a template–anchor perspective, they can be normally classified into two typical types: tail and reaction wheel (The limbs can be treated as multiple tails) [38]. So far, many existing terrestrial robots have been equipped with planar reorientation or spatial reorientation capability by using either the tail or wheel(s), as shown in Table I. Planar reorientation, i.e., reorienting the robot along a single Degree of Freedom (DoF), is relatively simple and has been extensively studied [7]–[23]. Spatial reorientation is more challenging because most of spatial reorientation tasks are essentially underactuated control where the number of actuated DoFs is less than the three DoFs to be controlled, e.g., the robots [26]–[28] only have a 2-DoF actuated tail but need to control 3D body orientation. In this paper, we aim at achieving underactuated spatial reorientation (regulating body yaw, pitch, and roll in falling) by using the tail and wheels together, which *exploits efficient Moment of Inertia (MoI) inducing capability of the tail and unlimited Range of Motion (RoM) feature of the wheel*. Since this is the first time to have such a hybrid inertial appendage for spatial reorientation in terrestrial robots, we give a brief review on the history of using inertial appendages in the following and elaborate the motivation at the same time.

A. Previous Work

TABLE I: Terrestrial Robots with Inertial Appendages

Robots	App. Types	Controlled DoFs	App. DoFs	Limited RoM[a]
[7]–[17]	Tail	1 (Pitch)	1	Yes
[18]–[23]	Tail	1 (Yaw or Roll)	1	No
[24], [25]	Tail	1 (Roll)	2	Yes
[26]–[28]	Tail	3 (Y., P., and R.)	2	Yes
[29]–[31]	Tail	3 (Y., P., and R.)	$\gg 2$	Yes
[32]	Wheel	1 (P.)	1	No
[33]	Wheel	2 (P. and R.)	2	No
[34]	Wheel	2 (P. and R.)	3	No
[35]	Wheel	3 (Y., P., and R.)	3	No
Ours	**Tail-Wheel**	**3 (Y., P., and R.)**	**2**	**No**

[a]Implying the potential collision between the appendage and the body

An extensive literature review on the tail-inspired robotic platforms has been conducted [7]–[31], see Table I. In terms of the number of the actuated DoFs, they can be classified into simple 1-DoF tails [7]–[23], 2-DoF actuated tails [24]–[28], and high-DoF continuum tails [29]–[31]. From a functional perspective, the robots [7]–[17] used their 1-DoF actuated tails to create pitch motion for correcting their body orientation in the sagittal plane; the legged robots [20]–[23] used the 1-DoF tail to create yaw motion for rapid turning; the legged robots

Manuscript received: May 17, 2023; Revised: Aug 17, 2023; Accepted: Sept 12, 2023. This paper was recommended for publication by Editor Xinyu Liu. This work was supported in part by Chow Yuk Ho Technology Centre of Innovative Medicine, The Chinese University of Hong Kong, in part by the Multiscale Medical Robotics Centre, AIR@InnoHK, and in part by the Research Grants Council (RGC) of Hong Kong under Grant 14209118, 14209719, and 14211320. All authors are with the Department of Mechanical and Automation Engineering, The Chinese University of Hong Kong, Hong Kong, China. (*Corresponding author: K. W. Samuel Au*)

IEEE Robotics and Automation Letters (RA-L) paper, presented at ICRA 2024, Yokohama, Japan. Cite as RA-L paper.

IEEE Robotics and Automation Letters (RA-L) paper, presented at ICRA 2024, Yokohama, Japan. Cite as RA-L paper.

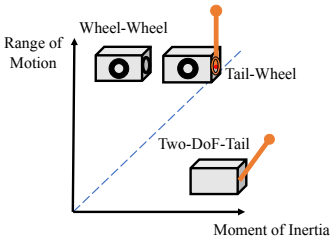

Fig. 1: Moment of Inertia (MoI) v.s. Range of Motion (RoM) for three templates with spatial reorientation capability: the wheel-wheel, tail-wheel, and two-DoF-tail robots. All templates have two DoFs of control input and are able to regulate three DoFs of body orientation in free falling with the principle of angular momentum conservation. The MoI of the tail-wheel robot can be larger than that of the wheel-wheel robot since the tail can induce a larger MoI than the wheel given the same mass (or has more efficient MoI-inducing) according to [38]. The RoM of the tail-wheel robot is greater than that of the two-DoF-tail robot due to the potential collision with the body of the two-DoF tail (see Fig. 5). Moreover, the rolling tail in the tail-wheel robot also enjoys unlimited RoM in the air.

[24], [25] used the 2-DoF tail to stabilize the frontal plane (i.e., body roll) by swinging the tail in a cone; the robots [26]–[28] used their 2-DoF actuated tails and the robots [29]–[31] used their continuum tails to stabilize their 3D body orientation. The tails were mostly subject to the limited RoM due to collision with their bodies, except for the planar inertial tails with reorientation capability along the yaw or roll DoF.

Unlike tails, (reaction) wheels have not been frequently applied to terrestrial robots for reorientation, although they are commonly-used in spacecraft [36]. [32] used a reaction wheel to stabilize body pitch during the flight phase for a jumping quadruped robot. [33] used two single-DoF wheel-type appendages to stabilize 2-DoF body attitude including pitch and roll. [34] proposed the agile ground robot AGRO consisting of four independently steerable wheels. [35] designed the robot Cubli which can balance and jump up, with the help of three flying wheels mounted on principal axes. Overall, the (reaction) wheels in terrestrial robots can easily provide planar reorientation capability, but it may not be an effective way to achieve spatial reorientation capability. For example, the improvement on the wheel architecture is necessary for AGRO to have four independently steerable wheels and appending three flying wheels as in Cubli requires extra design efforts.

Besides, a formal comparison between the tails and wheels has been conducted [38]. Specifically, [38] developed a comparative framework for planar reorientation by using different actuated inertial appendages. A metric, effectiveness of describing the planar inertia reorientation capability, was proposed. It was concluded that the tail can provide high values of effectiveness, while the reaction wheel can provide unlimited RoM during a longer time period. Not surprisingly, these results match the selection guideline while people use tails and wheels in their terrestrial robots [26]. To enjoy the wheel's unlimited RoM and the tail's efficient MoI-inducing, we combine both into one platform for enabling spatial reorientation capability (Fig. 1). In this paper, we specifically focus on a wheeled mobile robot appended by a simple tail, i.e., a hybrid tail-wheel robot. Moreover, it is underactuated (miss of yaw control capability) since the wheels serve as a virtual reaction wheel with pitch control capability while the tail has roll control capability. Although this type of robot has been used in previous work [15]–[18], such as *Tailbot* and *Dima*, they were only able to achieve planar reorientation and did not enable spatial reorientation using the wheels and tail together.

Spatial reorientation control for an underactuated hybrid tail-wheel robot is not a trivial problem. One of the challenges arises from online controller design for a dynamical underactuated system evolving for a fraction of a second. First, this challenge excludes open-loop methods. For example, [36] solved spacecraft attitude control with articulated appendages and reaction wheels by planning open-loop trajectories. It works well for a space robot with a long time horizon, but it is not suitable for *rapid* (a fraction of a second) spatial reorientation. Therefore, feedback control solutions were investigated. In the past, only a few methods were proposed to achieve spatial reorientation with a two-DoF tail. For example, in [26], the body orientation error was converted to an angle-axis representation and then the tail torque was commanded such that the body angular velocity was parallel to the Euler axis. However, the initial tail orientation required selection by optimization, thus the method was sensitive to initial states. [27] released the requirement on the initial orientation and designed an augmented controller, but it was specific to the two-DoF tailed robot. Another challenge is input limitation. For underactuated systems, input constraints complicate online controller design. In literature, such a constrained control problem has been studied in a few specific systems like nonholonomic mobile robots [40] and space robots [41], but few results are related to *rapid* 3D orientation/attitude control. Therefore, an online underactuated controller considering input constraints is needed to enable spatial reorientation rapidly.

B. Contributions

In this paper, our contributions are summarized as follows:

1) To our best knowledge, it is the first time to propose combining the tail and reaction wheel for underactuated spatial reorientation. The resulting hybrid tail-wheel robot enjoys benefits from the tail (efficient MoI-inducing) and the wheel (unlimited RoM). Its 1-DoF rolling tail also enjoys unlimited RoM in the air and its wheels act as a reaction wheel without extra attachment.
2) A novel metric-based Quadratic Programming (QP) is proposed, which enables online underactuated spatial reorientation for the hybrid tail-wheel robot while simultaneously accommodating appendage velocity constraints. The proposed QP allows us to conduct performance comparisons among three templates in Fig. 1 and emphasize the tail-wheel appendage's advantages of convergence performance and free of collision.
3) Experiments are conducted based on a newly-designed tail-wheel robot in a fraction of a second to demonstrate the effectiveness of the hybrid tail-wheel appendage and control algorithm.

II. Robot Overview

To show the combination, a tail-wheel robot is built, consisting of a rolling tail and four wheels (Fig. 2). The tail is directly

IEEE Robotics and Automation Letters (RA-L) paper, presented at ICRA 2024, Yokohama, Japan. Cite as RA-L paper.

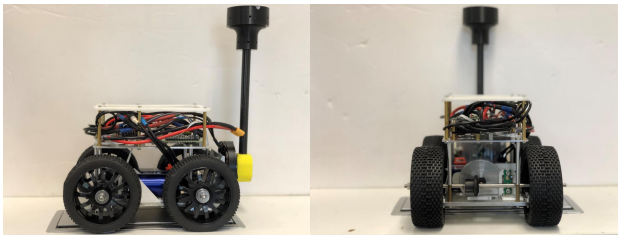

Fig. 2: Prototype of the underactuated hybrid tail-wheel robot.

driven by a SunnySky M8 brushless motor with a peak torque of 2 Nm. All four wheels are driven by a Traxxas' velineon 540xl motor with a peak torque of 0.12 Nm. It is rated for operation under a 4S LiPo battery of 16.8 V. The drive system has two gear stages, including a spur-pinion gear between the motor shaft and main shaft and a bevel gear system between the main shaft and wheel shaft. The overall drive ratio is 8:1. The motors are driven by a VESC motor controller (vesc-project.com). The robot parameters are in Table II.

The robot body is made of aluminum plates for its lightweight and durability. An LPMS-ME1 IMU provides the orientation of the robot in a quaternion form. The measurement of an accelerometer is used to detect a free fall. The angular position and velocity of the motors are measured by the magnetic encoder AS5047D. The software is implemented on a host PC (Intel(R) Core(TM) i7-8750H CPU @ 2.20GHz and 32GB RAM) and the generated codes in Simulink 2020b are uploaded to an onboard Raspberry Pi via a wireless network.

TABLE II: Robot Parameters

Body mass m_B	2.51 [kg]
Body inertia $\boldsymbol{I}_B^B$	diag([5.08,11.27,12.19]) $\times$ 10^{-3}[kg $\cdot$ m^2]
Wheel mass m_{W_i}	108 [g]
Wheel inertia $(\boldsymbol{I}_W)_{yy}$	1.63 $\times$ 10^{-4}[kg $\cdot$ m^2]
Wheel radius (r_W)	0.055 [m]
Tail mass m_T	300 [g]
Tail length ℓ_T	0.25 [m]
Body dimensions	0.21 [m] (L)$\times$0.12 [m] (W)$\times$0.10 [m] (H)

III. Modelling

The tail-wheel robot model consists of three parts: a rigid body, a tail, and four wheels. In Fig. 3, the point B denotes the Center of Mass (CoM) of the body and the frame $\{B\}$ is the body frame attached to it. The tail is assumed to be a long massless rod with a small point mass. The point T denotes the CoM of the tail and the frame $\{T\}$ is the tail frame. Four wheels are connected to the body and their CoMs are represented by W_i where $i = 1, ..., 4$. Moreover, they rotate with the same velocity. The frame $\{O\}$ denotes the inertial frame and the whole system CoM is assumed to locate at the origin of the inertial frame. All variables are given in Table III or depicted in Fig. 3.

In this paper, we focus on free-falling of the tail-wheel robot, thus the generalized coordinate can exclude the CoM position variables and keep the Euler angle of the body, wheel angle φ_1, and tail angle φ_2, i.e., $\boldsymbol{q} = [\boldsymbol{\theta}, \boldsymbol{\varphi}]^T$, where $\boldsymbol{\theta} = [\theta_1, \theta_2, \theta_3]^T$ and $\boldsymbol{\varphi} = [\varphi_1, \varphi_2]^T$. A reduced EoM describing the relation between the body Euler angle rate $\dot{\boldsymbol{\theta}}$ and appendage velocities $\dot{\boldsymbol{\varphi}}$ is available due to angular momentum

TABLE III: Nomenclature

m_B, m_T, m_{W_i}	Mass of the body, tail and i-th wheel, respectively
$\boldsymbol{H}^O$, $\boldsymbol{H}^B \in \mathbb{R}^3$	Total angular momentum expressed in the inertial frame and the body frame, respectively.
$\boldsymbol{H}_*^O \in \mathbb{R}^3$	Angular momentum expressed in the inertial frame. $* =$ body, tail, wheel.
$\boldsymbol{I}_*^O$, $\boldsymbol{I}_*^B \in \mathbb{R}^{3\times3}$	Moment of inertia of the body or the wheel expressed in the inertial frame and the body frame, respectively. $* = B, W_i$.
$\boldsymbol{I}_{W_i}^{W_i} \in \mathbb{R}^{3\times3}$	Moment of inertia of the wheel expressed in the wheel frame. $\boldsymbol{I}_{W_i}^{W_i} = \boldsymbol{I}_W$ is assumed and $\boldsymbol{I}_W = \text{diag}([(\boldsymbol{I}_W)_{xx}, (\boldsymbol{I}_W)_{yy}, (\boldsymbol{I}_W)_{zz}])$.
$\boldsymbol{\omega}_*^O$, $\boldsymbol{\omega}_*^B \in \mathbb{R}^3$	Angular velocity of the body frame or the wheel frame expressed in the inertial frame and the body frame, respectively. $* = B, W_i$.
$\boldsymbol{\rho}_*^O$, $\boldsymbol{\rho}_*^B \in \mathbb{R}^3$	Position of CoM expressed in the inertial frame and the body frame, respectively. $* = B, T, W_i$.
$\boldsymbol{\pi}_{XY}^Z \in \mathbb{R}^3$	Position vector from the point X to Y expressed in the frame $\{Z\}$.
$\theta_1, \theta_2, \theta_3$	Yaw, pitch, and roll, which are the rotation order.
φ_1, φ_2	Angular position of the wheel and tail, respectively
$\boldsymbol{R}_X^Y \in SO(3)$	Rotation matrix from the frame $\{X\}$ to $\{Y\}$, e.g., $\boldsymbol{\rho}_*^B = \boldsymbol{R}_O^B \boldsymbol{\rho}_*^O$ and $\boldsymbol{R}_B^O = (\boldsymbol{R}_O^B)^T$ hold.

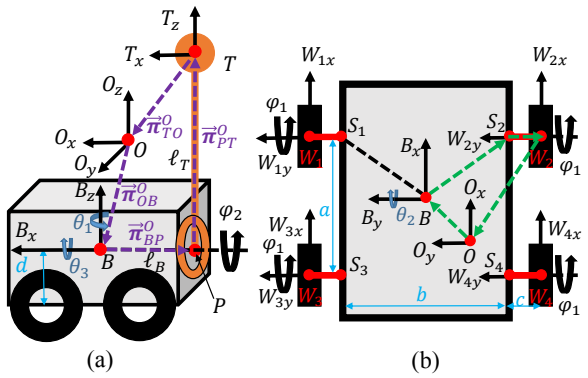

Fig. 3: Sketch of the underactuated hybrid tail-wheel robot. (a) Side view. (b) Top view.

conservation, assuming that the aerodynamics is ignored. To facilitate the control design of the systems with appendage velocity constraints, we will employ the reduced model.

To derive the reduced model, we start from an angular momentum equation expressed in the inertial frame

$$\boldsymbol{H}^O = \boldsymbol{H}_{Body}^O + \boldsymbol{H}_{Tail}^O + \boldsymbol{H}_{Wheel}^O, \tag{1}$$

where

$$\boldsymbol{H}_{Body}^O = \boldsymbol{I}_B^O \boldsymbol{\omega}_B^O + m_B \boldsymbol{\rho}_B^O \times \dot{\boldsymbol{\rho}}_B^O, \ \boldsymbol{H}_{Tail}^O = m_T \boldsymbol{\rho}_T^O \times \dot{\boldsymbol{\rho}}_T^O,$$
$$\boldsymbol{H}_{Wheel}^O = \Sigma_{i=1}^4 m_{W_i} \boldsymbol{\rho}_{W_i}^O \times \dot{\boldsymbol{\rho}}_{W_i}^O + \Sigma_{i=1}^4 \boldsymbol{I}_{W_i}^O \boldsymbol{\omega}_{W_i}^O.$$

It can be also expressed in the body frame

$$\begin{aligned}\boldsymbol{H}^B = \boldsymbol{I}_B^B \boldsymbol{\omega}_B^B + \Sigma_{i=1}^4 \boldsymbol{I}_{W_i}^B \boldsymbol{\omega}_{W_i}^B + m_B \boldsymbol{R}_O^B \boldsymbol{\rho}_B^O \times \dot{\boldsymbol{\rho}}_B^O \\ + m_T \boldsymbol{R}_O^B \boldsymbol{\rho}_T^O \times \dot{\boldsymbol{\rho}}_T^O + \Sigma_{i=1}^4 m_{W_i} \boldsymbol{R}_O^B \boldsymbol{\rho}_{W_i}^O \times \dot{\boldsymbol{\rho}}_{W_i}^O.\end{aligned} \tag{2}$$

The different momentum components in (2) are computed. Let us start from the third term in (2). With $\boldsymbol{\rho}_B^O = \boldsymbol{R}_B^O \boldsymbol{\rho}_B^B$,

$$\dot{\boldsymbol{\rho}}_B^O = \dot{\boldsymbol{R}}_B^O \boldsymbol{\rho}_B^B + \boldsymbol{R}_B^O \dot{\boldsymbol{\rho}}_B^B$$

holds. Thus, we have

$$m_B \boldsymbol{R}_O^B \boldsymbol{\rho}_B^O \times \dot{\boldsymbol{\rho}}_B^O = -m_B [\boldsymbol{\rho}_B^B \times][\boldsymbol{\rho}_B^B \times] \boldsymbol{\omega}_B^B + m_B \boldsymbol{\rho}_B^B \times \dot{\boldsymbol{\rho}}_B^B, \tag{3}$$

where $\boldsymbol{R}(\boldsymbol{x} \times \boldsymbol{y}) = (\boldsymbol{R}\boldsymbol{x}) \times (\boldsymbol{R}\boldsymbol{y})$ and $[\boldsymbol{\omega}_B^B \times] = \boldsymbol{R}_O^B \dot{\boldsymbol{R}}_B^O$ are used. $[(\cdot)\times]$ denotes a skew-symmetric matrix operator.

IEEE Robotics and Automation Letters (RA-L) paper, presented at ICRA 2024, Yokohama, Japan. Cite as RA-L paper.

Similarly, we calculate the last two terms on the right side of (2). Then we can update (2) to

$$\boldsymbol{H}^B = \boldsymbol{A}\boldsymbol{\omega}_B^B + \boldsymbol{B}\dot{\boldsymbol{\varphi}}, \quad \boldsymbol{A} \in \mathbb{R}^{3\times3}, \quad \boldsymbol{B} \in \mathbb{R}^{3\times2}, \tag{4}$$

where

$$\begin{aligned}
\boldsymbol{A} &= \boldsymbol{I}_B^B - m_B[\boldsymbol{\rho}_B^B\times][\boldsymbol{\rho}_B^B\times] - m_T[\boldsymbol{\rho}_T^B\times][\boldsymbol{\rho}_T^B\times] \\
&\quad - \Sigma_{i=1}^4 m_{W_i}[\boldsymbol{\rho}_{W_i}^B\times][\boldsymbol{\rho}_{W_i}^B\times], \\
\boldsymbol{B}\dot{\boldsymbol{\varphi}} &= m_B[\boldsymbol{\rho}_B^B\times]\dot{\boldsymbol{\rho}}_B^B + m_T[\boldsymbol{\rho}_T^B\times]\dot{\boldsymbol{\rho}}_T^B \\
&\quad + \Sigma_{i=1}^4 m_{W_i}[\boldsymbol{\rho}_{W_i}^B\times]\dot{\boldsymbol{\rho}}_{W_i}^B + \Sigma_{i=1}^4 \boldsymbol{I}_{W_i}^B\boldsymbol{\omega}_{W_i}^B \\
&= \begin{bmatrix} 0 & \frac{\ell_T m_T(\ell_T m_B + 4\ell_T m_W - 4d m_W\cos\varphi_2)}{m_r} \\ 4(\boldsymbol{I}_W)_{yy} & -\frac{(\ell_B\ell_T\sin\varphi_2(m_B+4m_W)}{m_r} \\ 0 & \frac{(\ell_B\ell_T\cos\varphi_2(m_B+4m_W)}{m_r} \end{bmatrix}\dot{\boldsymbol{\varphi}},
\end{aligned}$$

and all wheels are assumed to be the same ($\boldsymbol{I}_{W_i}^{W_i} = \boldsymbol{I}_W$, $m_{W_i} = m_W$). The derivation details can be found in [43].

Assuming that the robot starts from rest, the relation between the body angular velocity and the appendage velocity can be derived as

$$\boldsymbol{\omega}_B^B = -\boldsymbol{A}^{-1}\boldsymbol{B}\dot{\boldsymbol{\varphi}}. \tag{5}$$

Therefore, with the relation $\boldsymbol{\omega}_B^B = \boldsymbol{Q}\dot{\boldsymbol{\theta}}$, the reduced model is given by

$$\dot{\boldsymbol{\theta}} = \boldsymbol{J}\dot{\boldsymbol{\varphi}}, \quad \boldsymbol{J} \in \mathbb{R}^{3\times2}, \tag{6}$$

where

$$\boldsymbol{J} = -(\boldsymbol{A}\boldsymbol{Q})^{-1}\boldsymbol{B}, \quad \boldsymbol{Q} = \begin{bmatrix} -\sin\theta_2 & 0 & 1 \\ \cos\theta_2\sin\theta_3 & \cos\theta_3 & 0 \\ \cos\theta_2\cos\theta_3 & -\sin\theta_3 & 0 \end{bmatrix},$$

$\boldsymbol{J}$ acts like a Jacobian matrix, and $\boldsymbol{Q}$ is invertible if $\theta_2 \neq \pm(2k-1)\frac{\pi}{2}, k \in \mathbb{N}_0$. For simplicity, we assume $\boldsymbol{Q}$ is invertible. Note that the Jacobian-like matrix $\boldsymbol{J}$ is different from that in redundant robotic systems in terms of dimension.

IV. Underactuated Spatial Reorientation Method

Mathematically, a Quadratic Programming (QP) problem can be defined as

$$\begin{aligned} \min_{\boldsymbol{z}} \quad & \frac{1}{2}\boldsymbol{z}^T\boldsymbol{H}\boldsymbol{z} + \boldsymbol{g}^T\boldsymbol{z} + c \\ \text{s.t.} \quad & \boldsymbol{D}_{in}\boldsymbol{z} \preceq \boldsymbol{b}_{in} \end{aligned} \tag{7}$$

where $\boldsymbol{z} \in \mathbb{R}^n$ is a decision vector, $\boldsymbol{H} \in \mathbb{R}^{n\times n}$, $\boldsymbol{g} \in \mathbb{R}^n$, and $c \in \mathbb{R}$. $\boldsymbol{D}_{in} \in \mathbb{R}^{p\times n}$, $\boldsymbol{b}_{in} \in \mathbb{R}^p$ denote p inequality constraints.

A. Naive QP

From (6), we are able to achieve spatial reorientation on the body by properly manipulating the wheels and the tail together. A naive idea, often employed in redundant robotic systems, is to construct an optimization problem that minimizes the difference between the desired Euler angle rate $\dot{\boldsymbol{\theta}}_r \in \mathbb{R}^3$ and the actual Euler angle rate $\boldsymbol{J}\dot{\boldsymbol{\varphi}}$

$$\begin{aligned} \min_{\dot{\boldsymbol{\varphi}}} \quad & ||\dot{\boldsymbol{\theta}}_r - \boldsymbol{J}\dot{\boldsymbol{\varphi}}||^2 \\ \text{s.t.} \quad & \dot{\boldsymbol{\varphi}}_{min} \preceq \dot{\boldsymbol{\varphi}} \preceq \dot{\boldsymbol{\varphi}}_{max}, \end{aligned} \tag{8}$$

where $\dot{\boldsymbol{\varphi}}_{min} \prec 0$ and $\dot{\boldsymbol{\varphi}}_{max} \succ 0$ are lower and upper bounds, respectively.

When not considering the velocity constraints on $\dot{\boldsymbol{\varphi}}$, we can have an analytical solution. By converting the cost in (8) into a quadratic function as in (7), we have

$$\frac{1}{2}\dot{\boldsymbol{\varphi}}^T\boldsymbol{H}\dot{\boldsymbol{\varphi}} + \boldsymbol{g}^T\dot{\boldsymbol{\varphi}} + c = \dot{\boldsymbol{\varphi}}^T\boldsymbol{J}^T\boldsymbol{J}\dot{\boldsymbol{\varphi}} - 2\dot{\boldsymbol{\theta}}_r^T\boldsymbol{J}\dot{\boldsymbol{\varphi}} + \dot{\boldsymbol{\theta}}_r^T\dot{\boldsymbol{\theta}}_r, \tag{9}$$

where $\boldsymbol{H} = 2\boldsymbol{J}^T\boldsymbol{J}$, $\boldsymbol{g} = -2\boldsymbol{J}^T\dot{\boldsymbol{\theta}}_r$, $c = \dot{\boldsymbol{\theta}}_r^T\dot{\boldsymbol{\theta}}_r$. According to Section 9.1.1, [42], the optimal solution is

$$\dot{\boldsymbol{\varphi}}^* = -\boldsymbol{H}^{-1}\boldsymbol{g} = (\boldsymbol{J}^T\boldsymbol{J})^{-1}\boldsymbol{J}^T\dot{\boldsymbol{\theta}}_r. \tag{10}$$

For $\dot{\boldsymbol{\theta}}_r$, a common controller is

$$\dot{\boldsymbol{\theta}}_r = \dot{\boldsymbol{\theta}}_d + \boldsymbol{K}(\boldsymbol{\theta}_d - \boldsymbol{\theta}) = \boldsymbol{K}(\boldsymbol{\theta}_d - \boldsymbol{\theta}), \tag{11}$$

where $\boldsymbol{\theta}_d$ is assumed to be a constant desired body orientation and $\boldsymbol{K} \succ 0$. However, the resulting optimal control command $\dot{\boldsymbol{\varphi}}^*$ cannot achieve spatial reorientation (e.g., regulating the 3D body orientation to zero) for any configuration since ***non-zero*** $\dot{\boldsymbol{\theta}}_r$ may be parallel to the null space of $\boldsymbol{J}^T \in \mathbb{R}^{\mathbf{2\times3}}$, see (10). Once parallel, the control command $\dot{\boldsymbol{\varphi}}^*$ becomes zero, and thus the control authority is lost. In other words, the spatial reorientation task fails because the non-zero error exists.

B. Metric-based QP

It is natural to define a metric that measures how far is the desired Euler angle rate from the null space. It is easy to obtain the null space based on the Singular Value Decomposition (SVD) of $\boldsymbol{J}$ or through $\frac{\boldsymbol{J}_1\times\boldsymbol{J}_2}{||\boldsymbol{J}_1\times\boldsymbol{J}_2||}$, where the matrix $\boldsymbol{J} = [\boldsymbol{J}_1\ \boldsymbol{J}_2]$ in (6) and $\boldsymbol{J}_1, \boldsymbol{J}_2 \in \mathbb{R}^3$. Specifically, its basis could be the unit singular vector associated with the zero singular value. For simplicity, such a unit vector is regarded as the *null space direction vector*, denoted as $\boldsymbol{n} \in \mathbb{R}^3$.

There are many different definitions of the metric; here, we select one geometric metric originated from [37]

$$\beta = \cos^{-1}\left(\frac{\boldsymbol{e}_\theta}{||\boldsymbol{e}_\theta|| + \epsilon_1} \cdot \frac{\boldsymbol{n}}{||\boldsymbol{n}||}\right) = \cos^{-1}\left(\frac{\boldsymbol{e}_\theta^T\boldsymbol{n}}{||\boldsymbol{e}_\theta|| + \epsilon_1}\right), \tag{12}$$

where ϵ_1 is a small positive value that ensures no division by zero. $\boldsymbol{e}_\theta = \boldsymbol{K}(\boldsymbol{\theta}_d - \boldsymbol{\theta})$ is an error vector, and is obtained from (11) assuming $\boldsymbol{\theta}_d$ to be constant.

Remark 1: $\beta \to 0$ means $\boldsymbol{e}_\theta$ (or $\dot{\boldsymbol{\theta}}_r$) becomes parallel to $\boldsymbol{n}$; the control command will approach to zero (see (10)) and the orientation error may exist, as mentioned in the naive QP.

Next, we will introduce how to use this metric to keep the control authority until spatial reorientation is achieved. With the metric β, we expect $\beta \to \frac{\pi}{2}$ since $\boldsymbol{e}_\theta$ becomes perpendicular to the null space direction vector $\boldsymbol{n}$ and in other words, $\dot{\boldsymbol{\theta}}_r$ is perpendicular to $\boldsymbol{n}$ assuming $\boldsymbol{\theta}_d$ to be constant. In this case, $\dot{\boldsymbol{\theta}}_r$ would not be undermined by the null space and thus the control command can keep what it is, see (10). Inspired by this, we propose a metric-based QP, and its optimal control is given by

$$\begin{aligned} \dot{\boldsymbol{\varphi}}' \in \underset{\dot{\boldsymbol{\varphi}}}{\text{argmin}} \quad & ||\dot{\boldsymbol{\theta}}_r - \boldsymbol{J}\dot{\boldsymbol{\varphi}}||^2 \\ \text{s.t.} \quad & \dot{\boldsymbol{\varphi}}_{min} \preceq \dot{\boldsymbol{\varphi}} \preceq \dot{\boldsymbol{\varphi}}_{max}, \end{aligned} \tag{13}$$

where

$$\dot{\boldsymbol{\theta}}_r = \boldsymbol{e}_\theta + k_\psi\boldsymbol{\psi},$$

$$\boldsymbol{\psi} = (\beta - \frac{\pi}{2})\frac{\boldsymbol{e}_\theta \times \boldsymbol{n}}{||\boldsymbol{e}_\theta \times \boldsymbol{n}|| + \epsilon_2},$$

ϵ_2 is a small positive value, $k_\psi \neq 0$, and $\boldsymbol{\psi}$ is an augmented desired Euler angle rate which is perpendicular to both $\boldsymbol{e}_\theta$ and $\boldsymbol{n}$. $\boldsymbol{\psi}$ would not compete with $\boldsymbol{e}_\theta$ and keep the authority of reducing the error. The cross product operation has been used like in [27]; however, the usage was heavily dependent on the simplified model of the two-DoF-tail robot and thus cannot

IEEE Robotics and Automation Letters (RA-L) paper, presented at ICRA 2024, Yokohama, Japan. Cite as RA-L paper.

Algorithm 1 Metric-based QP

Result: The 3D body orientation converges to the desired state $\boldsymbol{\theta}_d$. In other words, spatial reorientation is achieved.

Initialization: set the initial state $\boldsymbol{\theta}_0$, desired constant state $\boldsymbol{\theta}_d$, threshold σ, sampling time Δt, and $k = 1$

if $\boldsymbol{e}_\theta^1(\boldsymbol{\theta}_0, \boldsymbol{\theta}_d) \in null[(\boldsymbol{J}^T)^1]$ **then**

  set $\dot{\boldsymbol{\varphi}}^1$ as a constant vector

  $\dot{\boldsymbol{\theta}}^1 = \boldsymbol{J}^1 \dot{\boldsymbol{\varphi}}^1, \quad \boldsymbol{\theta}^2 = \boldsymbol{\theta}^1 + \dot{\boldsymbol{\theta}}^1 \cdot \Delta t, \quad k = k + 1$

end

while $||\boldsymbol{\theta}_d^k - \boldsymbol{\theta}^k|| > \sigma$ **do**

  $\dot{\boldsymbol{\theta}}_r^k = \boldsymbol{e}_\theta^k + k_\psi \boldsymbol{\psi}^k$

  $\dot{\boldsymbol{\varphi}}^k = \underset{\dot{\boldsymbol{\varphi}}_{min} \preceq \dot{\boldsymbol{\varphi}}^k \preceq \dot{\boldsymbol{\varphi}}_{max}}{\text{argmin}} \quad (\dot{\boldsymbol{\theta}}_r^k - \boldsymbol{J}^k \dot{\boldsymbol{\varphi}}^k)^T (\dot{\boldsymbol{\theta}}_r^k - \boldsymbol{J}^k \dot{\boldsymbol{\varphi}}^k)$

  $\dot{\boldsymbol{\theta}}^k = \boldsymbol{J}^k \dot{\boldsymbol{\varphi}}^k, \ \boldsymbol{\theta}^{k+1} = \boldsymbol{\theta}^k + \dot{\boldsymbol{\theta}}^k \cdot \Delta t, \ k = k + 1$

end

be used in our tail-wheel robot. What we want to emphasize is, our design is more general since the null space direction vector $\boldsymbol{n}$ is determined from a systematic and generic method, SVD. With this advantage, the proposed QP is not system-specific and applicable to the two-DoF-tail robot and wheel-wheel robot, because their reduced models show the same architecture (governed by a Jacobian-like matrix) as that of our tail-wheel robot. Moreover, the proposed QP allows us to have a comparative study on inertial appendages for spatial reorientation, which has not been attained because of the lack of a unified orientation control design for different templates.

C. Physical Implementation

The metric-based QP algorithm for the hybrid tail-wheel robot is presented in Algorithm 1. Within it, $(\cdot)^k$ means the variable at the k-th step. The first step is to check if $\boldsymbol{e}_\theta$ is exactly in the null space. If so, the control command obtained from the metric-based QP is zero, and a constant vector will be assigned to the control command $\dot{\boldsymbol{\varphi}}^1$ such that $\boldsymbol{e}_\theta$ is not parallel to $\boldsymbol{n}$. After the first-step check, the formulation (13) is solved and the control command will be generated by the *off-the-shelf* QP solver (e.g., MATLAB's *quadprog*). The algorithm stops until the error between the current state and the desired state is less than the given threshold σ.

TABLE IV: Parameters in Simulation Section

Parameters	Values	Parameters	Values	Units
m_B	2.50	m_T	0.20	[kg]
$m_{W,side}$	0.10	$m_{W,back}$	0.20	[kg]
ℓ_T	0.20	ℓ_B	0.15	[m]
a	0.15	b	0.15	[m]
c	0.03	d	0.05	[m]
$(\boldsymbol{I}_B^B)_{xx}$	6.80	$(\boldsymbol{I}_B^B)_{yy}$	10.40	$\times 10^{-3}$[kg · m^2]
$(\boldsymbol{I}_B^B)_{zz}$	130.00	$(\boldsymbol{I}_W)_{yy}$	1.44	$\times 10^{-4}$[kg · m^2]

$m_{W,side}$ denotes the mass of the wheels in the tail-wheel robot or the wheel mounted on the side in the wheel-wheel robot, while $m_{W,back}$ denotes the wheel mounted on the back in the wheel-wheel robot.

V. Simulation

In this section, we will implement the proposed metric-based QP to show its effectiveness in MATLAB. To further show the advantage of the hybrid tail-wheel robot on both MoI and RoM, we will conduct a series of spatial reorientation tasks on wheel-wheel, two-DoF-tail, and tail-wheel robots. Their parameters in simulation are listed in Table IV.

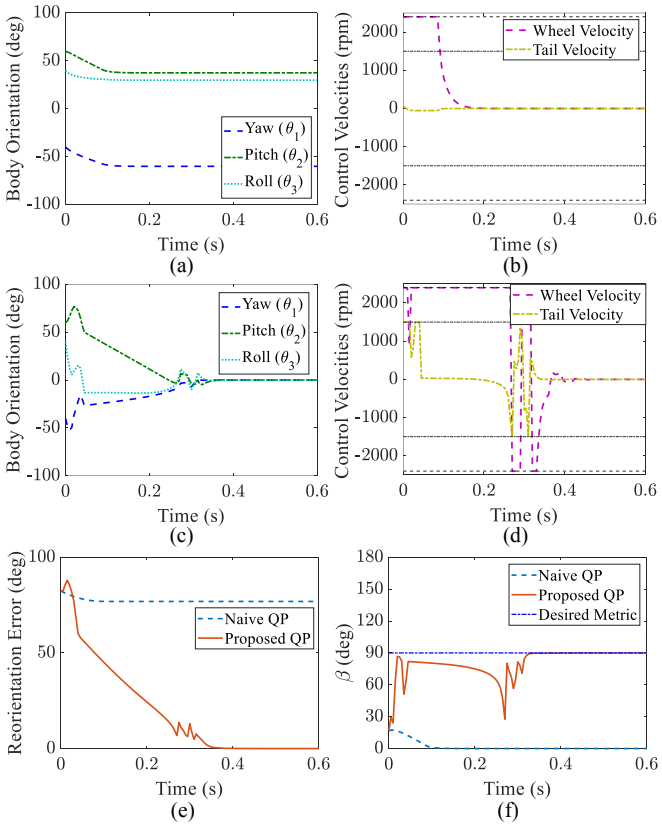

Fig. 4: Simulation results of spatial reorientation using the naive QP (a-b) and the proposed metric-based QP (c-d). (a,c) Evolution of body orientation. (b,d) Evolution of control velocities of both the wheels and the tail. Black dashed lines denote velocity constraints. (e) Reorientation error over time. (f) The geometric metric over time.

A. Algorithm Verification

To validate the process of spatial reorientation, the tail-wheel robot was dropped from a certain height. During this process, only the wheels and tail can affect the change of body orientation according to the angular momentum conservation principle. Fig. 4 shows one simulation example where the body orientation started from $[-40^\circ \ 60^\circ \ 40^\circ]^T$ and was expected to reach the origin. The simulation parameters $\boldsymbol{K} = k\boldsymbol{E}_{3\times3} = 65\boldsymbol{E}_{3\times3}$, $k_\psi = -165$, $\Delta t = 0.005$, and $\epsilon_1 = \epsilon_2 = 10^{-6}$ were used. From Figs. 4 (c) and (e), all Euler angles converged to zero, and the reorientation error ($||\boldsymbol{\theta}_d - \boldsymbol{\theta}||$) fell down to zero. In Fig. 4 (d), the control velocities of the wheel and tail respected the limitation as follows: $-2400 \leqslant \dot{\varphi}_1 \leqslant 2400$ rpm, $-1500 \leqslant \dot{\varphi}_2 \leqslant 1500$ rpm. Moreover, although there was an adjustment at 0.27 s, the metric could converge to 90°, which demonstrates its effectiveness of keeping control authority.

What we want to emphasize is that the proposed metric-based QP overcomes the limitation of the naive QP. Under the same simulation conditions, it is observed that the spatial reorientation task failed with a large reorientation error (the

IEEE Robotics and Automation Letters (RA-L) paper, presented at ICRA 2024, Yokohama, Japan. Cite as RA-L paper.

dashed blue line in Fig. 4 (e)). Note that the metric fell down to zero, i.e., $\beta \to 0^\circ$, which implies $\boldsymbol{e}_\theta$ has been parallel to $\boldsymbol{n}$. In other words, the control authority was lost when using the naive QP, whereas the metric-based QP was able to keep it ($\beta \to 90^\circ$), see Fig. 4 (f).

B. Performance Comparisons

Since the proposed QP is not specific to one system, we are allowed to conduct performance comparisons among wheel-wheel, two-DoF-tail, and tail-wheel robots (see sketches in Fig. 1). The reduced models of the wheel-wheel and two-DoF-tail robots can be derived as in Section III and are omitted in this paper for brevity. For the wheel-wheel robot, a wheel mounted on the back and aligned with the roll axis was used to replace the tail of the tail-wheel robot with the same mass ($m_{W,back}$) and the diameter close to the body height (selected as 0.12 m, thus its moment of inertia is 3.6×10^{-4} kg $\cdot$ m^2). For the two-DoF-tail robot, the tail parameters are the same as those in the tail-wheel robot, but the tail has two DoFs. While airborne, the full swinging of the tail was mechanically forbidden [27]. Specifically, the tail pitch and yaw ranges were $[-90^\circ, 90^\circ]$ and $[-180^\circ, 180^\circ]$, respectively. The rest of robot parameters and the appendage velocity limitation were the same. To cover various initial configurations, we selected eight initial states $\boldsymbol{\theta}_0 = [\pm 60^\circ, \pm 60^\circ, \pm 60^\circ]^T$ and the appendages started from zero position. The simulation duration was set as 0.6 s, which means all robots were dropped from around 1.76 meters. For each type, the control gains were carefully tuned for improving overall performance.

TABLE V: Performance Comparison Among Three Robots

Robot Types	k	k_ψ	$Er(^\circ)$	$T_c(s)$	N
(a) Wheel-Wheel	70	-150	$\mathbf{13.225 \pm 9.802}$	$\mathbf{1.279 \pm 0.512}$	0/8
(b) Two-DoF-Tail	50	-30	0.000 ± 0.000	0.268 ± 0.008	$\mathbf{8/8}$
(c) Tail-Wheel	50	-150	0.020 ± 0.017	0.589 ± 0.027	0/8

Fig. 5 shows the results of $\boldsymbol{\theta}_0 = [60^\circ, -60^\circ, 60^\circ]^T$. At 0.6 s, the wheel-wheel robot failed to achieve spatial reorientation, while both the two-DoF-tail and tail-wheel robots succeeded. In terms of appendage evolution, we found the two-DoF-tail robot violated the tail pitch and yaw limitation. Table V collected the results of eight cases, where Er denotes the body reorientation error at 0.6 s, T_c denotes the converging time when the body reorientation error is less than 0.02°, and N denotes the number of violating the physical ranges of the appendages. At 0.6 s, the wheel-wheel robot suffered from a large stabilization error and required a twofold converging time on average compared to the hybrid tail-wheel robot. This was because MoI of a wheel is normally smaller than that of a tail, given the same mass and wheel radius restriction [38]. Although the two-DoF-tail robot achieved the tasks very quickly and almost no error can be observed at 0.6 s, it violated the physical appendage range every time (8/8), which is infeasible in hardware. Once the appendage is subject to limited RoM, the collision between the body and the appendage is potential if no specific collision constraints are imposed. Overall, the results in the last row imply that the hybrid tail-wheel appendage enjoys the tail's efficient MoI-inducing and the wheel's unlimited RoM feature, thus its reorientation capability is highly enhanced without any physical collision in the air.

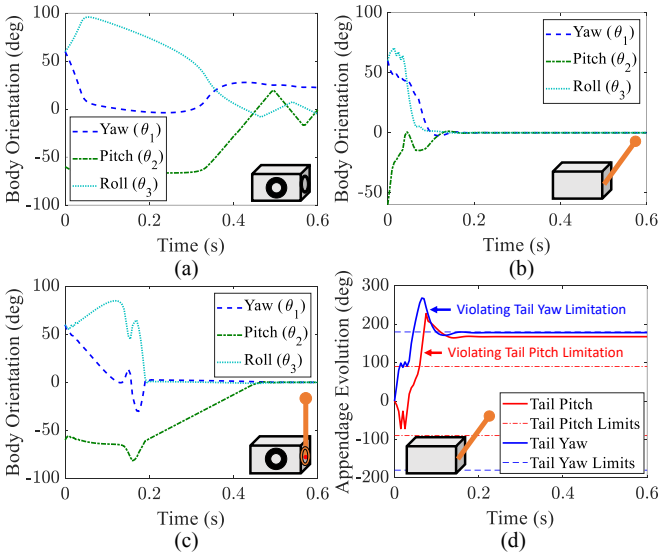

Fig. 5: Performance comparison on conducting spatial reorientation among three robots. (a-c) Body orientation evolution of the wheel-wheel robot, two-DoF-tail robot, and tail-wheel robot, respectively. (d) Appendage evolution of the two-DoF-tail robot.

VI. Experimental Validation

A. Experiment Setup

Experiments were designed to validate the spatial reorientation capability of the underactuated hybird tail-wheel robot in falling (see Fig. 9). In the dropping tests, the robot was dropped from a height of around 1.7 meters and the dropping duration was around 0.59 seconds. While dropping, the tail was pointing upward at the initial moment.

B. Experimental Results

Fig. 6 shows the results of one spatial reorientation trial using the proposed metric-based QP. The initial yaw, pitch, and roll angles were -21.97°, -23.55°, and -36.61°, respectively. The control parameters $\boldsymbol{K} = \text{diag}([275, 125, 125])$, $k_\psi = -400$, and $\epsilon_1 = \epsilon_2 = 10^{-6}$ were used. With our controller, the robot orientation can be righted to the neighborhood of the desired zero configuration before the impact. Specifically, the impact configuration was $[2.76^\circ \;\; 1.24^\circ \;\; -0.77^\circ]^T$. The drop was recorded by two cameras and the snapshots were displayed in Fig. 9. As shown in Fig. 6 (b), the control velocities were bounded by the saturation limitations, although some overshoots on the wheel velocity were observed. Those overshoots may be caused by the gear transmission mechanism, but they were still in the range of physical limitation if we set a relatively conserved saturation. As predicted, the geometric metric was forced to approach 90°. At the end of the spatial reorientation, an adjustment in the metric starting from 0.49 s can be observed. This was because the error was still non-zero and the adjustment was required.

IEEE Robotics and Automation Letters (RA-L) paper, presented at ICRA 2024, Yokohama, Japan. Cite as RA-L paper.

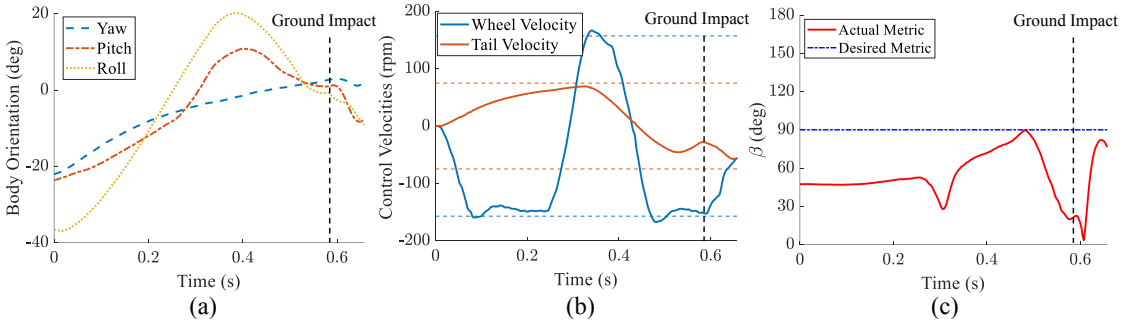

Fig. 6: Experimental results of spatial reorientation using the proposed metric-based QP. (a) Evolution of body orientation. (b) Evolution of control velocities of both the wheels and the tail. Dashed lines denote velocity constraints. (c) Evolution of the metric.

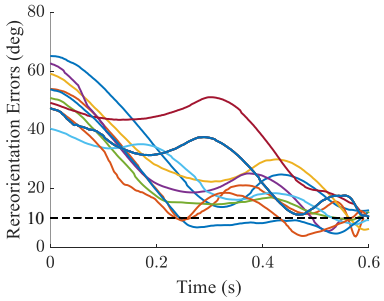

Fig. 7: Experimental results of reorientation errors using the proposed metric-based QP at 10 trials with different initial configurations.

Many trials have been conducted. The robot was dropped from different initial configurations. Overall, with the proposed algorithm, the robot achieved spatial reorientation, as shown in Fig. 7 (10 trials). The reorientation errors were in the range of $10^\circ \pm 5^\circ$ by the moment of the ground impact, which is acceptable in practice when considering body yaw, pitch, and roll together.

To show the incapability of the naive QP on spatial reorientation, the robot was dropped from a configuration close to the previous one in Fig. 6. The results were displayed in Fig. 8. The controlled pitch and roll showed the tendency of approaching to zero; however, the yaw DoF, which was underactuated, showed a large error. This was because the control authority was almost lost due to the use of the naive QP and this can be demonstrated by the evolution of the geometric metric, i.e., approaching to zero with fluctuations.

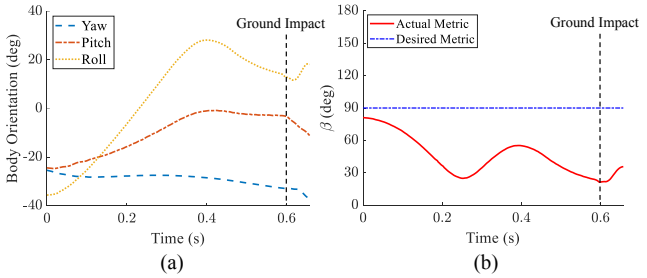

Fig. 8: Experimental results of the robot reorientation using the naive QP. (a) Evolution of body orientation. (b) Evolution of the metric.

VII. Discussions

Although the proposed algorithm in this paper starts from a specific prototype, it can be applicable to many different robot structures. The inspiration is twofold. First, to achieve spatial reorientation with underactuation, the usage of inertial appendages can be various. For example, compliant legs in RHex [38] can provide pitch authority, which is similar to the wheels we used. Recently, more and more legged robots with extra wheel(s) have been proposed, such as Ascento [6], Ollie [7], and SpaceBok [32]. Making use of the existing wheels while airborne can further reinforce robots' control capability on pitch, such as in Ascento and Ollie. Inspired by the success of our prototype, attaching a simple extra tail along the roll DoF to those legged robots has the potential of enabling spatial reorientation. Of course, the special case of potentially hitting the ground while landing needs to be further addressed. Second, the proposed control algorithm is not limited by the actuated DoF distribution studied in this paper (with pitch and roll control capability). To enable spatial reorientation with underactuation, the distribution of appendages can be flexible. Any pair selected from yaw, pitch, and roll DoFs is available for the proposed algorithm, e.g., pitch and yaw control capability in the two-DoF-tail robot.

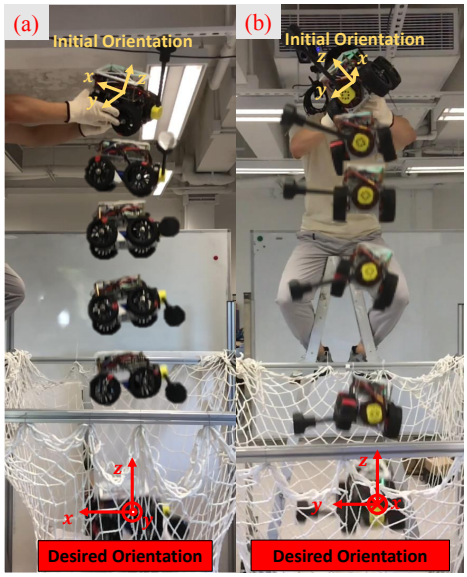

Fig. 9: Snapshots of one trial using the metric-based QP. Initial yaw, pitch, and roll angles were -21.97°, -23.55°, and -36.61°, respectively. (a) In the side view, the stabilization of the **pitch** DoF along the y-axis was observed. (b) In the back view, the stabilization of the **yaw** DoF along z-axis and the **roll** DoF along x-axis was observed.

IEEE Robotics and Automation Letters (RA-L) paper, presented at ICRA 2024, Yokohama, Japan. Cite as RA-L paper.

VIII. Conclusion and Future Work

In this paper, we proposed to enable underactuated spatial reorientation with two classical types of inertial appendages, the tail and reaction wheel, by using a novel metric-based QP. Different from previous work mainly focusing on either one of those appendages, the resulting hybrid tail-wheel robot combines two core abilities, unlimited RoM and efficient MoI-inducing. Besides, the proposed algorithm is crucial in underactuated spatial reorientation, where the two-DoF velocity-limited control input can regulate three-DoF states. In the simulation, the proposed QP was verified, and the performance comparison emphasized the advantages of the combined tail-wheel appendage on spatial reorientation (small convergence error, relatively fast convergence speed, and free of collision in the air), which cannot be attained by either tails or reaction wheels. In experiments, we further demonstrated the real-time spatial reorientation capability of the hybrid appendage by multiple dropping tests. In the future, we are interested in applying the metric to other optimization frameworks, e.g., a Model Predictive Control (MPC) framework, and extending the algorithm to the case of non-zero total angular momentum.

References

[1] Jonah Siekmann et al., "Blind Bipedal Stair Traversal via Sim-to-Real Reinforcement Learning," *Robotics: Science and Systems*, p17, 2021.

[2] Justin K. Yim et al., "Precision Robotic Leaping and Landing Using Stance-phase Balance," *IEEE RA-L*, Vol. 5, No. 2, pp. 3422-3429, 2020.

[3] Daniel J. Gonzalez, Mark C. Lesak, Andres H. Rodriguez, Joseph A. Cymerman, and Christopher M. Korpela, "Dynamics and Aerial Attitude Control for Rapid Emergency Deployment of the Agile Ground Robot AGRO," *IEEE/RSJ IROS*, pp. 2577-2584, 2020.

[4] Nikita Rudin, Hendrik Kolvenbach, Vassilios Tsounis, and Marco Hutter, "Cat-Like Jumping and Landing of Legged Robots in Low Gravity Using Deep Reinforcement Learning," *IEEE Trans. on Rob.*, Vol. 38, No. 1, pp. 317-328, 2022.

[5] Benjamin Katz, Jared Di Carlo, and Sangbae Kim, "Mini Cheetah: A platform for Pushing the Limits of Dynamic Quadruped Control," *IEEE Inter. Conference on Robotics and Automation*, pp. 6295-6301, 2019.

[6] Victor Klemm, Alessandro Morra, Ciro Salzmann, Florian Tschopp, Karen Bodie, Lionel Gulich, Nicola Küng, Dominik Mannhart, Corentin Pfister, Marcus Vierneisel, Florian Weber, Robin Deuber, and Roland Siegwart, "Ascento: A Two-Wheeled Jumping Robot," *IEEE International Conference on Robotics and Automation*, pp. 7515-7521, 2019.

[7] Shuai Wang, Leilei Cui, Jingfan Zhang, Jie Lai, Dongsheng Zhang, Ke Chen, Yu Zheng, Zhengyou Zhang, and Zhong-Ping Jiang, "Balance Control of a Novel Wheel-legged Robot: Design and Experiments," *IEEE Inter. Conference on Robotics and Automation*, pp. 6782-6788, 2021.

[8] Avik De and Daniel E. Koditschek, "Parallel composition of templates for tail-energized planar hopping," *IEEE ICRA*, pp. 4562-4569, 2015.

[9] Avik De et al., "The Penn Jerboa: A Platform for Exploring Parallel Composition of Templates," *Technical Report to Accompany*, 2016.

[10] Guan-Horng Liu, Hou-Yi Lin, Huai-Yu Lin, Shao-Tuan Chen, and Pei-Chun Lin, "A Bio-Inspired Hopping Kangaroo Robot with an Active Tail," *Journal of Bionic Engineering*, Vol. 11, No. 4, pp. 541-555, 2014.

[11] Aaron M. Johnson, Thomas Libby, Evan Chang-Siu, Masayoshi Tomizuka, Robert J. Full, and D. E. Koditschek, "Tail assisted dynamic self righting," *Int. Conf. on Clim. and Wal. Rob.*, pp. 611-620, 2012.

[12] Knut Graichen, Sebastian Hentzelt, Alexander Hildebrandt, Nadine Kärcherc, Nina Gaißertc, and Elias Knubbenc, "Control design for a bionic kangaroo," *Control Eng. Practice*, Vol. 42, pp. 106-117, 2015.

[13] Anna L. Brill et al., "Tail-assisted rigid and compliant legged leaping," *IEEE/RSJ Int. Conf. on Intel. Rob. and Sys.*, pp. 6304-6311, 2015.

[14] Jianguo Zhao, Tianyu Zhao, Ning Xi, Fernando J. Cintrón, Matt W. Mutka, and Li Xiao, "Controlling aerial maneuvering of a miniature jumping robot using its tail," *IEEE/RSJ IROS*, pp. 3802-3807, 2013.

[15] Evan Chang-Siu, Thomas Libby, Masayoshi Tomizuka, and Robert J. Full, "A lizard-inspired active tail enables rapid maneuvers and dynamic stabilization in a terrestrial robot," *IEEE/RSJ IROS*, pp. 1887-1894, 2011.

[16] Thomas Libby, Talia Y. Moore, Evan Chang-Siu, Deborah Li, Daniel J. Cohen, Ardian Jusufi and Robert J. Full, "Tail-assisted pitch control in lizards, robots and dinosaurs," *Nature*, vol. 481, pp. 181-184, 2012.

[17] Amir Patel and M. Braae, "Rapid Acceleration and Braking: Inspirations from the Cheetah's Tail," *IEEE ICRA*, pp. 793-799, 2014.

[18] Amir Patel and M. Braae, "Rapid turning at high-speed: Inspirations from the cheetah's tail," *IEEE/RSJ IROS*, pp. 5506-5511, 2013.

[19] Jusufi A, Kawano DT, Libby T, and Full RJ, "Righting and turning in mid-air using appendage inertia: reptile tails, analytical models and bio-inspired robots," *Bioinspiration & Biomim.*, Vol. 5, p. 045001, 2010.

[20] Carlos Casarez, Ivan Penskiy, and Sarah Bergbreiter, "Using an inertial tail for rapid turns on a miniature legged robot," *IEEE/RSJ International Conference on Intelligent Robots and Systems*, pp. 5469-5474, 2013.

[21] A.O. Pullin, N.J. Kohut, D. Zarrouk, and R. S. Fearing, "Dynamic turning of 13 cm robot comparing tail and differential drive," *IEEE Inter. Conference on Robotics and Automation*, pp. 5086-5093, 2012.

[22] HyunGyu Kim, Kyungmin Jeong, Metin Sitti and TaeWon Seo, "Steering control of a water-running robot using an active tail," *IEEE/RSJ Inter. Conf. on Intelligent Robots and Systems*, pp. 4945-4950, 2016.

[23] Wael Saab and Pinhas Ben-Tzvi, "Maneuverability and Heading Control of a Quadruped Robot Utilizing Tail Dynamics," *ASME Proceedings: Unmanned, Ground and Surface Robotics*, Vol. 7, 2017.

[24] Garrett Wenger, Avik De and Daniel E. Koditschek, "Frontal Plane Stabilization and Hopping with a 2DOF Tail," *IROS*, pp. 567-573, 2016.

[25] Amir Patel and Edward Boje, "On the Conical Motion of a Two-Degree-of-Freedom Tail Inspired by the Cheetah," *IEEE Transactions on Robotics*, vol. 31, no. 6, pp. 1555-1560, 2015.

[26] Randall Briggs et al, "Tails in biomimetic design: Analysis, simulation, and experiment," *IEEE IROS*, pp. 1473-1480, 2012.

[27] Evan Chang-Siu, Thomas Libby, Matthew Brown, Robert J. Full and Masayoshi Tomizuka, "A nonlinear feedback controller for aerial self-righting by a tailed robot," *Int. Con. on Rob. and Auto.*, pp. 33-39, 2013.

[28] Xiangyu Chu et al., "Null-Space-Avoidance-Based Orientation Control Framework for Underactuated, Tail-Inspired Robotic Systems in Flight Phase," *IEEE Robo. and Auto. Let.*, vol. 4, no. 4, pp. 3916-3923, 2019.

[29] W. S. Rone et al., "Design, Modeling, and Integration of a Flexible Universal Spatial Robotic Tail," *J MECH ROBOT.*, vol. 10, no. 4, 2018.

[30] W. Saab, W. S. Rone, A. Kumar and P. Ben-Tzvi, "Design and Integration of a Novel Spatial Articulated Robotic Tail," *IEEE/ASME Trans. Mechatronics.*, vol. 24, no. 2, pp. 434-446, 2019.

[31] W. S. Rone and P. Ben-Tsvi, "Continuum robotic tail loading analysis for mobile robot stabilization and maneuvering," in *Proc. ASME IDETC/CIE*, 2014, Art. no. 34678.

[32] H. Kolvenbach et al, "Towards Jumping Locomotion for Quadruped Robots on the Moon," *IEEE IROS*, pp. 5459–5466, 2019.

[33] Chong Hong, Dewei Tang, Qiquan Quan, Zhuoqun Cao, Che Wang, Metin Sitti, and Zongquan Deng, "Control of Two-Degree-of-Freedom Inertial Appendages of a Small-Scale Jumping Robot for Enhanced Terrestrial and Aerial Maneuverability," *IEEE/ASME Transactions on Mechatronics*, vol. 28, no. 3, pp. 1754-1765, 2023.

[34] Daniel J. Gonzalez1, Mark C. Lesak, Andres H. Rodriguez, Joseph A. Cymerman, and Christopher M. Korpela, "Dynamics and Aerial Attitude Control for Rapid Emergency Deployment of the Agile Ground Robot AGRO," *IEEE Int. Conf. on Intel. Rob. and Sys.*, pp. 2577–2584, 2020.

[35] Mohanarajah Gajamohan, Michael Merz, Igor Thommen and Raffaello D'Andrea, "The Cubli: A Cube that can Jump Up and Balance," *IEEE Int. Conf. on Intel. Rob. and Sys.*, pp. 3722–3727, 2012.

[36] C. Rui, I. V. Kolmanovsky, and N. H. McClamroch, "Nonlinear attitude and shape control of spacecraft with articulated appendages and reaction wheels," *IEEE Trans. on Auto. Con.*, vol. 45, no. 8, pp. 1455–1469, 2000.

[37] Y. Nakamura and R. Mukherjee, "Nonholonomic path planning of space robots," *IEEE Inter. Conf. on Rob. and Auto.*, pp. 1050-1055, 1989.

[38] Thomas Libby et al., "Comparative Design, Scaling, and Control of Appendages for Inertial Reorientation," *IEEE Transactions on Robotics*, vol. 32, no. 6, pp. 1380–1398, 2016.

[39] Bruno Siciliano, Lorenzo Sciavicco, Luigi Villani, and Giuseppe Oriolo, "Robotics: Modelling, Planning and Control," *Springer Publishing Company*, Chapter 2 and 3, 2008.

[40] Xiao Yu, Lu Liu, and Gang Feng, "Trajectory Tracking for Nonholonomic Vehicles with Velocity Constraints," *IFAC-PapersOnLine*, vol. 48, no. 11, pp. 918-923, 2015.

[41] P. Tsiotras and J. H. Luo, "Control of underactuated spacecraft with bounded inputs," *Automatica*, Vol. 36, pp. 1153-1169, 2000.

[42] S. Boyd and L. Vandenberghe, "Convex optimization," *Cambridge university press*, 2004.

[43] https://github.com/xiangyuchu03/Underactuated-Tail-Wheel-Robot.git

IEEE Robotics and Automation Letters (RA-L) paper, presented at ICRA 2024, Yokohama, Japan. Cite as RA-L paper.